frontiers | Frontiers in Chemistry

REVIEW
published: 25 April 2022
doi: 10.3389/fchem.2022.881518

Role of Anions in the Synthesis and Crystal Growth of Selected Semiconductors

*Shaidatul Najihah Matussin, Ashmalina Rahman and Mohammad Mansoob Khan**

Chemical Sciences, Faculty of Science, Universiti Brunei Darussalam, Gadong, Brunei

The ideal methods for the preparation of semiconductors should be reproducible and possess the ability to control the morphology of the particles with monodispersity yields. Apart from that, it is also crucial to synthesize a large quantity of desired materials with good control of size, shape, morphology, crystallinity, composition, and surface chemistry at a reasonably low production cost. Metal oxides and chalcogenides with various morphologies and crystal structures have been obtained using different anion metal precursors (and/or different sulfur sources for chalcogenides in particular) through typical synthesis methods. Generally, spherical particles are obtained as it is thermodynamically favorable. However, by changing the anion precursor salts, the morphology of a semiconductor is influenced. Therefore, precursors having different anions show some effects on the final forms of a semiconductor. This review compiled and discussed the effects of anions (NO_3^-, Cl^-, SO_4^{2-}, CH_3COO^-, $CH(CH_3)O^-$, etc.) and different sources of S^{2-} on the morphology and crystal structure of selected metal oxides and chalcogenides respectively.

Keywords: semiconductors, metal oxides, chalcogenides, shaped-dependent properties, Anion directed crystal growth

OPEN ACCESS

Edited by:
Wee-Jun Ong,
Xiamen University Malaysia, Malaysia

Reviewed by:
Quanjun Xiang,
University of Electronic Science and Technology of China, China
Metwally Madkour,
Kuwait University, Kuwait
Kezhen Qi,
Dali University, China
Lutfi Kurnianditia Putri,
Monash University Malaysia, Malaysia

****Correspondence:***
Mohammad Mansoob Khan
mmansoobkhan@yahoo.com
mansoob.khan@ubd.edu.bn

Specialty section:
This article was submitted to Photocatalysis and Photochemistry, a section of the journal Frontiers in Chemistry

Received: *22 February 2022*
Accepted: *31 March 2022*
Published: *25 April 2022*

Citation:
Matussin SN, Rahman A and Khan MM (2022) Role of Anions in the Synthesis and Crystal Growth of Selected Semiconductors. Front. Chem. 10:881518. doi: 10.3389/fchem.2022.881518

INTRODUCTION

Heterogeneous photocatalysis using semiconductors has drawn attention following the discovery of the Honda-Fujishima effect in 1972 (Liu et al., 2014). Photocatalysis has also gained remarkable attention due to its potential application for energy shortage and environmental issues which include hydrogen production from water (Shi et al., 2019), carbon dioxide reduction to fuels (M.S et al., 2021), and toxic pollutants removals in the environment (Koutavarapu et al., 2021). Semiconductor consists of a band structure in which the conduction band (CB) is separated from the valence band (VB) by a band gap. This is one of the important properties as it determines the light absorption and the redox capabilities of a semiconductor. Theoretically, in photocatalysis, when the energy of incident light is equal or larger than that of the band gap of a semiconductor, electrons (e^-) and holes (h^+) are generated in the CB and VB, respectively (Matussin et al., 2020a; Naidi et al., 2021; Rahman et al., 2021). These photogenerated charge carriers may be involved in the following possible processes:

1) Migrate to the surface-active sites of semiconductor
2) Captured by the defect sites in bulk and/or on the surface of the semiconductor
3) Recombine and release energy in the form of heat or photon

The last two processes are, however, considered to be deactivation processes due to these photogenerated e^- and h^+ would not involve in photocatalytic reactions. A large number of inorganic

semiconductors have been explored including metal oxides, IV group, III-V compounds, and metal chalcogenides. Semiconductor oxide nanomaterials-based photocatalysts have been recognized as one of the most promising areas of research and application such as TiO_2, ZnO, SnO_2, CeO_2, etc (Qi et al., 2013; Khan et al., 2017; Kowsari et al., 2017; Parwaiz et al., 2019; Matussin et al., 2020b; Rahman and Khan, 2021). Metal oxides are mainly used as photocatalysts due to their non-toxicity, low cost, stability, and resistance to photocorrosion.

In comparison to most of the metal oxides, semiconductors including III-V compounds, IV group, and metal chalcogenides show narrow band gap, large optical absorption coefficients, and broad-spectrum light collection (Popescu, 2006; Ahluwalia, 2017). They are called narrow-gap semiconductors in which the band gap of these semiconductors is usually less than 2.3 eV. This could allow light absorption at the wavelength of more than 540 nm. Chalcogenides are compounds consisting of at least one chalcogen anion (S^{2-}, Se^{2-} or Te^{2-}) and at least one electropositive element. Chalcogenides have drawn significant attention due to their great and highly demanded properties including narrow band gap energy, non-toxicity, and bio-compatibility.

The performance of a semiconductor is strongly correlated with its size. When the size of materials falls into the nanoscale, materials may exhibit different properties (Navya and Daima, 2016). As the size is reduced, the atoms or ions percentage exposed on the surface increases, resulting in an increase in the surface to volume ratio (Navya and Daima, 2016). Therefore, the number of active sites for catalytic reactions increases. Moreover, the reduction of size might also affect the electronic properties of the material. In particular, as the material size is smaller than its Bohr radius, the movement of the charge carriers is greatly confined in physical size due to the quantum confinements. This results in the discrete electronic band structure, leading to size-dependent electronic and optical properties (Li and Wu, 2015).

Furthermore, the morphology of a catalyst is crucial since factors such as the size and shape of particles, the energy associated with facets, coordination of atoms, and the presence of protective ligands can mainly influence its catalytic efficiency (Cao et al., 2016; Guo et al., 2018; Lin et al., 2019; Mishra and Nanda, 2020). In a recent study, Chiu et al. (2012) conducted facet-dependent catalytic activity of Au nanocubes, octahedral, and rhombic dodecahedra towards 4-nitroaniline. It was reported that anisotropic shape particles can alter the reaction performance due to differences in crystal facets exposed. Therefore, the concept of morphology-dependent catalytic and/or photocatalytic activity of a semiconductor has become a growing topic in catalysis and for the exploration of potential applications nowadays.

Varied shapes and sizes of semiconductors are reported to have been obtained through different synthesis methods for instance hydrothermal, precipitation, sol-gel, microwave, green synthesis, and many others (Qi et al., 2013; Sahay et al., 2013; Soren et al., 2015; Hasnidawani et al., 2016; Yin et al., 2016). Furthermore, counter-anion in the metal salts precursors plays a role in the shape-selective growth of semiconductor nanomaterials. It is said that the inorganic anions themselves might be selectively adsorbed on particular facets and thus greatly affect the size, and morphology of the nanomaterials (Herricks et al., 2004; Qi et al., 2014). To date, the lack of studies on anions effects on the development of metal oxides and chalcogenides have become a challenge to prepare metal oxides and chalcogenides with controlled morphology and size. Moreover, various shaped semiconductors without implementation of agents are somehow in demand to prevent high-cost methods and chemical hazards. Recently, researchers have gradually begun studies on the effects of anions on the production of semiconductors. Therefore, in this review, different morphologies of metal oxides and chalcogenides obtained using different metal salts precursors and their crystal growth are discussed in-depth. To the authors' knowledge, there has been no review on the development of semiconductors using different metal precursors having different anions. This is the first review and compilation of the role of anions in the synthesis and crystal growth of selected metal oxides and chalcogenides.

ANION DIRECTED SYNTHESIS OF METAL OXIDES

Metal oxides nanoparticles (NPs) have been widely exploited for many different areas such as toxic pollutants removal (Gowthaman et al., 2020; Yang et al., 2020; Zhou et al., 2021), drug delivery (He et al., 2019; Mallakpour et al., 2022), hydrogen production (Chen et al., 2015; Bhosale et al., 2016; Chen et al., 2018), CO_2 reduction (Loh and Kherani, 2019; Sun et al., 2021; Kuan et al., 2022), optoelectronics (C. Nehru et al., 2012; Jayakumar et al., 2022; Wang et al., 2010), etc., Controllable growth of metal oxides NPs with defined morphology such as spherical, rod-like, sheet-like, cubic amongst others have been synthesized and reported to have an influence on their catalytic properties.

Various morphologies of metal oxides have been acquired from different metal precursors salts (**Figure 1**). For instance, Panda *et al.* synthesized ZnO nanorods through a sonochemical method using two different Zn precursors namely: $Zn(CH_3COO)_2$ and $Zn(NO_3)_2{\cdot}6H_2O$ dissolved in a basic condition at room temperature using ammonium acetate and ammonia solution (Panda et al., 2013). Flower-like ZnO was obtained when NO_3^- anion precursor was used, while CH_3COO^- anion precursor showed a nanorod with an average width size between 150 and 500 nm for both anions. Similarly, Gusatti et al. (2011) prepared ZnO *via* the sonochemical method. However, $Zn(NO_3)_2{\cdot}6H_2O$ and $ZnCl_2$ were used. NaOH was added to both the solutions at 90°C resulting in a mixture of short nanoprisms and nanorods of 18.91 nm long and 11.50 nm wide for NO_3^- anion precursor and nanorods of 23 nm diameter for Cl^- anion precursor. High purity ZnO NPs were synthesized using $Zn(NO_3)_2{\cdot}6H_2O$, $Zn(CH_3COO)_2$, $ZnSO_4{\cdot}7H_2O$ and $ZnCl_2$ using a typical precipitation method as reported by Pourrahimi et al. (2014) The precursors' solutions were stirred at 60°C for 15 min and pre-heated NaOH was added to the solutions yielding star-shaped particle (500 nm) for NO_3^- anion,

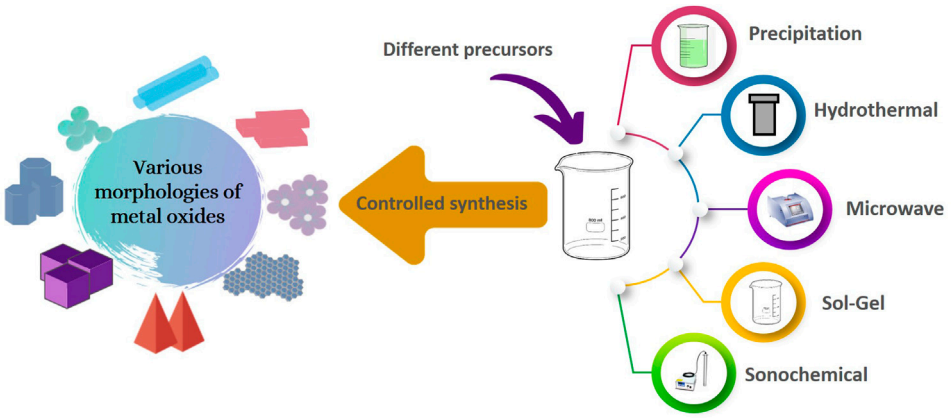

FIGURE 1 | Different morphologies of metal oxides synthesized using different precursors having different anions.

cone-shaped particle (25 nm) for CH_3COO^- anion, petal-like for both SO_4^- and Cl^- anions (80–100 nm).

The formation of hexamethylenetetramine (HMTA)-mediated ZnO nanoparticles was reported by van Rijt et al. (2020) The ZnO particles were synthesized using $Zn(NO_3)_2{\cdot}6H_2O$, $Zn(CH_3COO)_2$, $ZnSO_4{\cdot}7H_2O$ and $ZnCl_2$ through precipitation method. Hexamine was added to the solutions at 80°C for 6 h. Hexagonal pillar-like shape was obtained when NO_3^- anion was used, the dumbbell-shaped particle was seen for CH_3COO^- and hexagonally faceted plate-shaped particles were obtained for both SO_4^- and Cl^- anions. Kaenphakdee et al. (2022) prepared ZnO using $Zn(CH_3COO)_2$ and $Zn(NO_3)_2{\cdot}6H_2O$. Precipitation method was used in which monoethanolamine in 2-methoxy ethanol was added for CH_3COO^- anion precursor and hexamethylenetetramine in H_2O for NO_3^- anion precursor at 90°C for 2 h. These resulted in the aggregation of particles which yielded about 400–500 nm for CH_3COO^- anion precursor and submicron rod-shaped particle at about 3 µm in length and 500 nm in diameter for NO_3^- anion precursor. Kathalingam et al. (2015) synthesized various morphologies of ZnO by varying the zinc precursors ($Zn(NO_3)_2{\cdot}6H_2O$ and $Zn(CH_3COO)_2$) the precursor's concentration (10 mM- 0.5 M) as well as the preparation method. It was found that ZnO using NO_3^- anion precursor shows spherical (45 nm), rod-like (35 nm), plate-like (120 nm), needle-like (32 nm), tube-like (35 nm) ZnO particles. The concentration of the precursor solution was varied leading to different morphologies as well. ZnO particles using CH_3COO^- anion shows rod-like (15 nm) and wire-like structures (20 nm). Ozel et al. (2016) prepared ZnO particles using $Zn(NO_3)_2{\cdot}6H_2O$ and $ZnCl_2$ *via* hydrothermal method. NH_4OH was added to the precursor solution at 100°C. Flower-like structure of ZnO was obtained with an average size of 5–7 µm when NO_3^- anion precursor was used while rod-like ZnO was attained when Cl^- anion was used. Dey et al. (2021) reported on the precursor-dependent nanostructures of ZnO. $Zn(CH_3COO)_2$, $Zn(NO_3)_2{\cdot}6H_2O$ and, $ZnCl_2$ were used in the hydrothermal synthesis of ZnO at 120°C. Various morphologies of ZnO were obtained: nano-pencil, nanorods, and no defined shape for CH_3COO^-, NO_3^-, and Cl^- anions, respectively.

Different morphologies of CeO_2 were observed as reported by Wu et al. (2008) $CeCl_3{\cdot}7H_2O$ and $Ce(NO_3)_3{\cdot}6H_2O$ precursors were used in the hydrothermal reaction. The reaction was carried out at 140°C for 48 h producing CeO_2 nanorods (15–25 nm in diameter and length up to a few micrometers) and CeO_2 nanocubes (8–30 nm) for Cl^- and NO_3^- anions, respectively. Kumar et al. (2017) prepared mesoporous CeO_2 using $CeCl_3{\cdot}7H_2O$, $Ce(NO_3)_3{\cdot}6H_2O$, $(NH_4)_2Ce(NO_3)_6$ and $Ce(CH_3COO)_3$ through hydrothermal reaction. The reaction was carried out at different conditions for each precursor used. L-glycine and $Na_2(CO_2)_2$ solution were prepared and added to $CeCl_3$ solution and hydrothermally heated at 160°C. In the case of $Ce(CH_3COO)_3$, Hexadecylamine in ethanol was added to the solution and stirred at room temperature. It was then placed in an oven at 60°C for 2 days. For $Ce(NO_3)_3$, a mixture of CTAB and NaOH was added to $Ce(NO_3)_3$ solution and stirred at 90°C and aged at 60°C for 12 h. Acryl amide, glucose, ammonia solution were added to $(NH_4)_2Ce(NO_3)_6$ solution and it was stirred at room temperature for 5 h. Transamidation of acetamide with N-octylamine was carried out and investigated using the CeO_2 produced from these methods. It was found that CeO_2 with a rod-like structure produced the highest conversion of acetamide.

Samiee and Goharshadi (2012) reported on the effects of different precursors on the properties of CeO_2 in which CeO_2 was prepared using $Ce(NO_3)_3{\cdot}6H_2O$ and $(NH_4)_2Ce(NO_3)_6$ in a microwave-assisted synthesis. It was found that CeO_2 synthesized using $Ce(NO_3)_3{\cdot}6H_2O$ showed cubic-shaped particles with an average particle size of 7 nm. Similarly, CeO_2 synthesized using $(NH_4)_2Ce(NO_3)_6$ was also showed cubic structure with an average particle size of about 3 nm. Aneggi et al. (2014) reported on the shape-dependent activity of CeO_2 in soot combustion. Hydrothermal method was used to synthesize CeO_2 in a basic condition using NaOH. Two different precursors were used namely, $Ce(NO_3)_3{\cdot}6H_2O$ and $CeCl_3{\cdot}7H_2O$ in the synthesis producing CeO_2 nanocubes and

nanorods, respectively. The high stability of CeO_2 for the catalytic combustion of chlorobenzene was synthesized using various cerium precursors (Zhang et al., 2021). $Ce(NO_3)_3{\cdot}6H_2O$, $Ce(CH_3COO)_3$, $CeCl_3{\cdot}7H_2O$, and $Ce(SO_{34})_3{\cdot}8H_2O$ were used in hydrothermal synthesis at 180°C. It was observed that CeO_2 synthesized from $Ce(NO_3)_3{\cdot}6H_2O$, $Ce(CH_3COO)_3$, $CeCl_3{\cdot}7H_2O$ and $Ce(SO_{34})_3{\cdot}8H_2O$ show rod-like (5–11 nm in diameter and 40–250 nm in length), lamellar structured particles (3–11 nm), a series of small spherical particles (5–23 nm) and strip structured particles (70–75 nm in width and 70–950 nm in length), respectively. It was found that rod-like CeO_2 showed an increase in soot combustion activity.

Zhu et al. (2020) synthesized CeO_2 using $Ce(NO_3)_3{\cdot}6H_2O$ and $CeCl_3{\cdot}7H_2O$ in hydrothermal reaction for photocatalytic CO_2 reduction. The synthesis was carried out at 140 and 180°C producing CeO_2 nanocubes of about 30 nm length and nanorod of 200–400 nm in length and 20 nm in diameter when $Ce(NO_3)_3{\cdot}6H_2O$ and $CeCl_3{\cdot}7H_2O$ were used, respectively. It was observed that CeO_2 nanorods showed efficient photocatalytic CO_2 reduction. Feng *et al.* reported on highly reducible nanostructured CeO_2 for CO oxidation (Feng et al., 2018). Hydrothermal synthesis reaction was carried out using $Ce(NO_3)_3{\cdot}6H_2O$ and $CeCl_3{\cdot}7H_2O$ at 110 and 160°C, respectively. Tube-like CeO_2 was obtained with an average diameter of 30–70 nm and 1–5 μm in length for $Ce(NO_3)_3{\cdot}6H_2O$. Meanwhile, rod-like CeO_2 at about 300 nm to 1 μm in length and 20–40 nm in diameter was observed for $CeCl_3{\cdot}7H_2O$. The authors found that rod-like CeO_2 exhibited the highest activity. Aboul-Gheit et al. (2014) prepared shape-dependent nano-TiO_2 for the photodegradation of black b dye in water. TiO_2 was synthesized using $TiCl_4$ and $Ti(OCH(CH_3)_2)_4$ *via* precipitation method. Semisphere particles of about 20 nm were obtained when $TiCl_4$ was used whereas for the case of $Ti(OCH(CH_3)_2)_4$, highly agglomerated CeO_2 particles were obtained. Singh et al. (2017) synthesized TiO_2 *via* sol-gel method using $K_2TiO(C_2O_4)_2{\cdot}2H_2O$ and $Ti(OCH(CH_3)_2)_4$. NH_4OH was added to $K_2TiO(C_2O_4)_2{\cdot}2H_2O$ solution and stirred at room temperature and diethanolamine was added in the $Ti(OCH(CH_3)_2)_4$ solution. Irregular spherical to a mixture of platelet-shaped CeO_2 (11–53 nm) and spherical (29–58 nm) for $K_2TiO(C_2O_4)_2{\cdot}2H_2O$ and $Ti(OCH(CH_3)_2)_4$, respectively.

Influence of different anions precursors on the morphologies of Co_3O_4 was reported by Hussain et al. (2014) $Co(NO_3)_2{\cdot}6H_2O$, $CoCl_2{\cdot}6H_2O$, $Co(CH_3COO)_2{\cdot}4H_2O$ and $CoSO_4{\cdot}7H_2O$ were used in the synthesis in a low temperature aqueous chemical growth. It was found that the synthesized Co_3O_4 showed a honeycomb-like, network of nanowires, grass-like and nanosheets when $Co(NO_3)_2{\cdot}6H_2O$, $CoCl_2{\cdot}6H_2O$, $Co(CH_3COO)_2{\cdot}4H_2O$ and $CoSO_4{\cdot}7H_2O$ were used, respectively. Various Fe precursors of Fe were used to produce Fe_2O_3 as reported by Guru et al. (2016) Microwave synthesis was used at 100°C by mixing ethylene glycol. NaOH, CTAB, and Fe precursors namely: $Fe(NO_3)_3{\cdot}9H_2O$, $FeSO_4{\cdot}7H_2O$, $Fe_2(SO_4)_3{\cdot}H_2O$ and $FeCl_3{\cdot}6H_2O$. For all cases, spherical particles were obtained in which the average particle sizes were in the range of 19–80 nm. In another report, α-Fe_2O_3 was synthesized hydrothermally from three different Fe sources: $Fe(NO_3)_3{\cdot}9H_2O$, $FeCl_3{\cdot}6H_2O$ and $Fe(SO_4)_2{\cdot}6H_2O$ (Benhammada et al., 2020). Similarly, for all cases, spherical particles were observed giving an average particle size in the range of 80–110 nm (Sanjini et al., 2017). Microwave synthesized CuO NPs showed various morphologies when three different precursors were used. Spherical-shaped CuO NPs were obtained for the case of $CuCl_2$, needle-shaped CuO NPs were obtained for the case of $Cu(NO_3)_2$, and spherical particles for the case of $CuSO_4$.

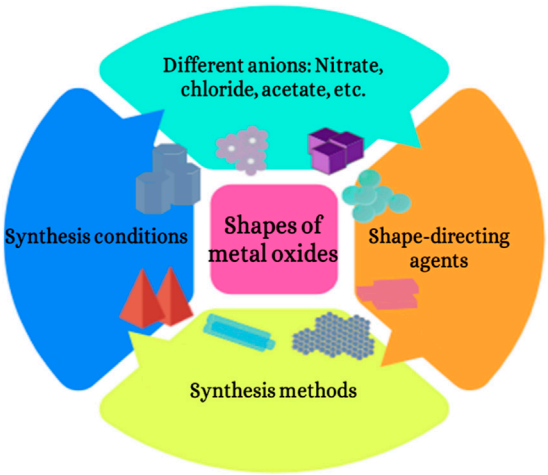

FIGURE 2 | Effect of synthesis conditions on the morphologies of metal oxides.

Counter anions have different abilities to electrostatically stabilize individual nanoparticles into isolated highly crystalline solids during the full course of the reaction as stated by Pourrahimi et al. (2014) In general, the formation of spherical particles is thermodynamically more favorable (Khodashenas and Ghorbani, 2019). Hence, spherical particles have mainly been observed and obtained in the literature. It is well known that the nucleation and growth of nanostructures can be achieved using stabilizing agents with desired thermodynamic and kinetic control. The shape-selectivity of a semiconductor is usually achieved by additional shape-directing agents. These agents absorb preferentially on specific crystallographic planes leading to the change of direction and rate of crystal growth (Jain et al., 2019). Moreover, synthesis methods also play a role in the shape-selectivity of a semiconductor (**Figure 2**). Although there are many reports on the role of various additives in controlling crystal growth, there are only a few studies reported the influence of inorganic counter ions in shape-selective growth of metal oxide without the involvement of agents (Siegfried and Choi, 2005).

In the case of a typical synthesis of metal oxides using Cl^- counter anion precursor, the final shape of a metal oxide (MO) is generally rod-like. This has been illustrated in many literatures as can be seen in **Table 1**. In general, when Cl^- counter anion precursor is used in the synthesis with NaOH, it forms $M(OH)_3$ (M = Zn, Ce, Ti, Co, Fe, and Cu) in which rod-like structure has been obtained. During the dehydration and oxidation process, the rod-like shape is not changed except for the size. It can be said

TABLE 1 | Various metal oxides synthesized using different precursors.

No	Materials	Precursors	Morphology and size	Phase	Applications	References
1	ZnO	i. $Zn(CH_3COO)_2$ ii. $Zn(NO_3)_2{\cdot}6H_2O$	i. Flower like (150–500 nm) ii. Nanorods (150—500 nm)	Hexagonal wurtzite	None	Panda et al. (2013)
2	ZnO	i. $Zn(NO_3)_2{\cdot}6H_2O$ ii. $ZnCl_2$	i. Mixture of nanoprisms and nanorods (length 18.91 nm and diameter 11.50 nm) ii. Nanorods (23 nm)	Hexagonal wurtzite	None	Gusatti et al. (2011)
3	ZnO	i. $Zn(NO_3)_2{\cdot}6H_2O$ ii. $Zn(CH_3COO)_2{\cdot}2H_2O$ iii. $ZnSO_4{\cdot}7H_2O$ iv. $ZnCl_2$	i. Star-shaped (500 nm) ii. Cone-shaped (25 nm) iii. Petal-like (80–100 nm) iv. Petal-like (80–100 nm)	Hexagonal wurtzite	None	Pourrahimi et al. (2014)
4	ZnO	i. $Zn(CH_3COO)_2{\cdot}2H_2O$ ii. $ZnCl_2$ iii. $Zn(NO_3)_2{\cdot}6H_2O$ iv. $ZnSO_4{\cdot}7H_2O$	i. Dumbbell-like ii. Hexagonally faceted plate-shaped iii. Hexagonal pillar-shaped iv. Hexagonally faceted plate-shaped	Hexagonal wurtzite	None	van Rijt et al. (2020)
5	ZnO	i. $Zn(CH_3COO)_2{\cdot}2H_2O$ ii. $Zn(NO_3)_2{\cdot}6H_2O$	i. Aggregration particles (400—500 nm) ii. Submicron rod-shaped (3 μm in length and 500 nm in diameter)	Hexagonal wurtzite	None	Pourrahimi et al. (2014)
6	ZnO	i. $Zn(CH_3COO)_2{\cdot}2H_2O$ ii. $Zn(NO_3)_2{\cdot}6H_2O$	i. Rod-like and wire-like (15—20 nm) ii. Spherical, rod-like, plate-like, needle-like and tube like (22–120 nm)	Hexagonal wurtzite	None	Kathalingam et al. (2015)
7	ZnO	i. $Zn(NO_3)_2{\cdot}6H_2O$ ii. $ZnCl_2$	i. Rod-like (0.5–1 μm) ii. Flower like (5–7 μm)	Hexagonal wurtzite	None	Ozel et al. (2016)
8	ZnO	i. $Zn(CH_3COO)_2{\cdot}2H_2O$ ii. $Zn(NO_3)_2{\cdot}6H_2O$ iii. $ZnCl_2$	i. Nanopencil ii. Nanorods iii. No defined shape	Hexagonal wurtzite	None	Dey et al. (2021)
9	CeO_2	i. $CeCl_3{\cdot}7H_2O$ ii. $Ce(NO_3)_3{\cdot}6H_2O$	i. Nanorods (15–25 nm diameters and lengths up to a few micrometers) ii. Cube-like (8–30 nm)	-	None	Wu et al. (2008)
10	CeO_2	i. $CeCl_3{\cdot}7H_2O$ ii. $Ce(NO_3)_3{\cdot}6H_2O$ iii. $Ce(CH_3COO)_3{\cdot}6H_2O$ iv. $(NH_4)_2Ce(NO_3)_6$	Mesoporous	Cubic	Transmidation of acetamide	Kumar et al. (2017)
11	CeO_2	i. $Ce(NO_3)_3{\cdot}6H_2O$ ii. $(NH_4)_2Ce(NO_3)_6$	i. Cubic (7.08 nm) ii. Cubic (3.37 nm)	Cubic	None	Samiee and Goharshadi, (2012)
12	CeO_2	i. $Ce(NO_3)_3{\cdot}6H_2O$ ii. $CeCl_3{\cdot}7H_2O$	i. Nanocubes ii. Nanorods	Cubic	Soot combustion	Aneggi et al. (2014)
13	CeO_2	i. $Ce(CH_3COO)_3$ ii. $Ce(SO_4)_3{\cdot}8H_2O$ iii. $Ce(NO_3)_3{\cdot}6H_2O$ iv. $CeCl_3{\cdot}7H_2O$	i. Lamellar (3–11 nm) ii. Almost spherical (5–23 nm) iii. Nanorods (5–11 nm diameter and length 40–250 nm) iv. Strip-like structure (70–75 nm	Cubic	Combustion of chlorobenzene	Zhang et al. (2021)
14	CeO_2	i. $CeCl_3{\cdot}7H_2O$ ii. $Ce(NO_3)_3{\cdot}6H_2O$	i. Nanorod (200–400 nm length and 20 nm diameter) ii. Nanocubes (30 nm)	-	CO_2 photoreduction	Zhu et al. (2020)
15	CeO_2	i. $CeCl_3{\cdot}7H_2O$ ii. $Ce(NO_3)_3{\cdot}6H_2O$	i. Tube-like (1–5 μm length- 30–70 nm diameters) ii. Rod-like (length of 300 nm to 1 μm and diameters of 20–40 nm)	Cubic	CO oxidation	Feng et al. (2018)
16	TiO_2	i. $TiCl_4$ ii. $Ti(OCH(CH_3)_2)_4$	Semisphere (20 nm)	Anatase	Photodegradation of black b dye	Aboul-Gheit et al. (2014)
17	TiO_2	i. $K_2TiO(C_2O_4)_2{\cdot}2H_2O$ ii. Ti $[OCH(CH_3)_2]_4$	i. Irregular spherical and platelet-like (11–53 nm) ii. Spherical with agglomeration (29–58 nm)	Anatase	None	Singh et al. (2017)
18	Co_3O_4	i. $CoCl_2{\cdot}2H_2O$ ii. $Co(NO_3)_2{\cdot}2H_2O$ iii. $(CH_3COO)_2CO{\cdot}4H_2O$ iv. $CoSO_4{\cdot}7H_2O$	i. Network of nanowires ii. Honey-comb like iii. Grass-like iv. Nanosheets	Cubic	pH sensor	Hussain et al. (2014)
19	Fe_2O_3	i. $FeSO_4{\cdot}7H_2O$ ii. $Fe_2(SO_4)_3{\cdot}H_2O$ iii. $Fe(NO_3)_3{\cdot}9H_2O$ iv. $FeCl_3{\cdot}6H_2O$	i. Spherical (19.4–46.7 nm) ii. Spherical (29.1–67.6 nm) iii. Spherical (29.1–40.8 nm) iv. Spherical (29.1–80 nm)	-	None	Guru et al. (2016)
20	Fe_2O_3	i. $FeCl_3{\cdot}6H_2O$ ii. $Fe(NO_3)_3{\cdot}9H_2O$ iii. $Fe(SO_4)_2{\cdot}6H_2O$	i. Spherical (110 nm) ii. Spherical (90 nm) iii. Spherical (80 nm)	Rhomboedral hematite	Thermal decomposition of cellulose	Benhammada et al. (2020)
21	CuO	i. $CuCl_2$ ii. $CuNO_3$ iii. $CuSO_4$	i. Spherical ii. Needle shape iii. Spherical	Monoclinic	Methylene blue degradation	Sanjini et al. (2017)

that nanorod-like geometry is the intrinsic formation of the case of Cl^- (C. Nehru et al., 2012; Kaenphakdee et al., 2022; Dey et al., 2021). Apart from that, Cl^- directs the growth of particles into tube-like or wire-like particles. This is similar to rod-like structure however, the synthesis conditions such as temperature, acidity, and basicity as well as the use of capping agents leads to the distortion of the rod shape of particles (Samiee and Goharshadi, 2012; Zhu et al., 2020; Zhang et al., 2021).

Interestingly, when NO_3^- salts were introduced, the morphology of the metal oxides was directed into faceted shaped MO (cube, plate-like, hexagonal, honeycomb, etc.) (C. Nehru et al., 2012; Jayakumar et al., 2022; Wang et al., 2010; Panda et al., 2013; Zhu et al., 2020). Typically, metal oxides form polyhedral-kind of shape and in order to tune the surface free energies and induce the anisotropic growth of well-shaped nanostructures, adscititious surfactants are required in which this is the case for most of the reported shapes (**Table 1**) (Yang and Gao, 2006). However, a dissolution-recrystallization process under the strong basic condition would influence the production of cube-like or faceted metal oxides particles (Yang and Gao, 2006).

Pourrahimi et al. (2014) has conducted studies on the probable "shielding effect" of different counter anions on the particle stabilization. It was found that both Cl^- and NO_3^- ions showed inability to stabilize the particles. Furthermore, nitrate-based precursor has shown to produce smaller particles which was aimed to grow specific directional morphologies in hydroxide solutions (Cho et al., 2008). On the other hand, CH_3COO^- ions has the strong ability to stabilize as it has been suggested to originate from strong uni- and bi-dentate oxygen coordination bonding of the acetate ions to individual metal atoms, or parallel bridging of the two oxygen atoms in the CH_3COO^- ions to positively charged metal atoms of the particles (Sun et al., 2007; Segets et al., 2011; Pourrahimi et al., 2014). Moreover, Nicholas et al. (2012) stated that, partially positively charged methyl functional unit of the CH_3COO^- ions associated with the insufficiently condensed negatively charged metal hydroxide which therefore suggesting the stabilization of growing nanoparticles probably derived from a formed amphiphilic capping layer around the particle (Pourrahimi et al., 2014).

Spherical-shaped CeO_2 has shown high efficiency in photocatalysis activities due to its small particle size and high surface areas (Sanjini et al., 2017; Benhammada et al., 2020). However, nanoshaped CeO_2 (cube, rod, hexagonal, etc.) are evident to have effects on photocatalysis activities. This is because nanoshaped CeO_2 enabled the study of the correlation between exposed surfaces and photocatalytic activities. Anneggi *et al.* proposed that {100}/{110} exposed surfaces are more reactive in photocatalysis activities, particularly on CO oxidation. This observation can be seen in many studies (Kumar et al., 2017; Feng et al., 2018; Zhu et al., 2020; Zhang et al., 2021).

ANION DIRECTED SYNTHESIS OF CHALCOGENIDES

Chalcogenides are narrow-band gap semiconductors consisting of at least one chalcogen anion (sulphide, selenide, or telluride) and at least one more electropositive element (Khan and Khan, 2021; Rahman and Khan, 2021). Unlike metal oxide, researchers have widely explored varying the sulfur precursors for chalcogenides instead of varying the anions of the metal precursors. **Table 2** shows some of the reported works on varying the precursors of selected chalcogenides. Over the last decades, many preparation routes have been developed for the synthesis of chalcogenides with different morphologies, particle sizes, and crystal structures that can be obtained from different raw materials through different synthetic pathways (**Figure 3**). Various authors have investigated the effect of anion on the morphology, particle size, and crystal structure of different chalcogenides. For instance, Gaur and Jeevanandam (2015) investigated the effect of anions (acetate, chloride, nitrate, and sulfate) in diphenyl ether and in solid-state that leads to the formation of CdS nanoparticles with different morphologies. The CdS nanoparticles derived from solid-state thermal decomposition of the cadmium-thiourea complexes with acetate, chloride, nitrate, and sulfate ions exhibited spheres, nanotubes, nanoflowers, and irregular morphologies, respectively. On the other hand, thermal decomposition of the cadmium thiourea complexes with acetate, chloride, and nitrate ions in diphenyl ether results in CdS nanoparticles with microspheres, nanopyramids, and a mixture of nanoparticles and nanorods morphologies, respectively. Amongst the synthesized materials, CdS synthesized from cadmium acetate and thiourea *via* solid-state exhibited the highest photocatalytic crystal violet degradation of 99.2%.

In a different study, two morphologies of MoS_2 were obtained by using thiourea and L-cysteine as sulfur sources (Zhang et al., 2017). Zhang *et al.* reported that MoS_2 prepared by using thiourea had a petal-shaped structure, and the crystal size was larger while MoS_2 prepared from L-cysteine had a loose structure, and the crystal size was smaller. They also reported that MoS_2 prepared from thiourea exhibited better catalytic performance than that from L-cysteine in the hydrodeoxygenation reaction. Hydrothermal assisted synthesis of CdS/MoS_2 using three different sulfur sources; thioacetamide, L-cysteine, and thiourea has been reported by Wang et al. (2018) Their results showed that the different sulfur sources induced differences in crystallization, morphology, elemental composition, and absorption in the UV–visible light region. Among the three sulfur sources, CdS/MoS_2 prepared using thioacetamide showed excellent adsorption performance and the highest photocatalytic ability to degrade methylene blue with approximately 97% within 120 min under visible light irradiation, much higher than that achieved by CdS/MoS_2 prepared using L-cysteine and thiourea.

Kim et al. (2016) have successfully controlled the morphology of ZnS by utilizing anionic precursors *via* a hydrothermal method for reduction of Cr(VI). The authors reported rate of nucleation is the main factor affecting the morphology variations, and it mainly depends on the rate of release of S^{2-} by the anionic thiourea, thioacetamide, and sodium sulfide precursors. When thiourea and thioacetamide are used as the sulfur sources, the rate of S^{2-} release is slow compared to that achieved with sodium sulfide. The rate of release of S^{2-} from thiourea, in particular, is

TABLE 2 | Summary of previous work on the effect of anions on the morphology, particle size, and crystal structure of various chalcogenides.

No	Materials	Metal precursors	Sulfur precursors	Morphology and size	Crystal phase	Application	References
1	CdS synthesized *via* thermal decomposition	Cadmium acetate Cadmium chloride Cadmium nitrate Cadmium sulfate	Thiourea	Cadmium acetate: spheres with diameter ~100–200 nm Cadmium Chloride: nanotubes with diameter ~70–100 nm Cadmium nitrate: nanoflowers with diameter ~150–200 nm Cadmium sulfate: irregular morphologies	Hexagonal and cubic	Photocatalytic degradation of crystal violet	Gaur and Jeevanandam, (2015)
2	MoS_2 synthesized *via* silica sol method	$(NH_4)_6Mo_7O_{24}{\cdot}4H_2O$	Thiourea L-cysteine	Thiourea: nanowires with high crystallinity L-cysteine: nanowires with poor crystallinity	2H-MoS_2	Hydro-deoxygenation	Zhang et al. (2017)
3	ZnS synthesized *via* spray pyrolysis	$ZnCl_2$	Thiourea Thioacetamide	Small clusters with average size of 80–100 nm	Wurtzite	-	Zeng et al. (2013)
4	CdS/MoS_2 synthesized *via* hydrothermal method	$CdCl_2{\cdot}2H_2O$ $Na_2MoO_4{\cdot}2H_2O$	Thiourea L-cysteine Thioacetamide	Thiourea: granular in shape L-cysteine: spherical porous structure Thioacetamide: rod-like and flower-like Thiourea: cauliflower-like morphology with an average diameter of 0.8–1 μm	Both the cubic and hexagonal phases of CdS were present	Photocatalytic degradation of methylene blue	Wang et al. (2018)
5	ZnS synthesized *via* hydrothermal method	$Zn(CH_3COO)_2{\cdot}6H_2O$	Thiourea, Sodium sulfide nonahydrate, Thioacetamide	Sodium sulfide: rice grain-shaped microstructures with size of 15–20 mm long, 1–2 mm thick and 2–5 mm wide Thioacetamide: roughly hedge apple-like shape with an average diameter of approximately 1–2 μm.	Cubic	Laser-induced reduction of Cr(VI)	Kim et al. (2016)
6	ZnS synthesized via chemical bath deposition	$ZnSO_4$ $ZnCl_2$	Thiourea Thioacetamide Sodium thiosulfate Sodium sulfide	- $FeSO_4{\cdot}7H_2O$: short nanorods having length up to 500 nm and diameter within 40–100 nm	Wurtzite Sphalerite	-	Kozhevnikova et al. (2020)
7	FeS_2 synthesized *via* solvothermal method	$FeSO_4{\cdot}7H_2O$ $FeCl_3$ $Fe(NO_3)_39H_2O$	Thiourea	$FeCl_3$: large nanowires (>90%) along with some micro-rods $Fe(NO_3)_3{\cdot}9H_2O$: nanowires with diameter in the range 40–60 nm and length up to tens of μm Thioacetamide: Ni_3S_2 nanorods and small MoS_2 nanosheets	Cubic pyrite	-	Kar and Chaudhuri, (2004)
8	MoS_2/Ni_3S_2 synthesized *via* hydrothermal method	$Na_2MoO_42H_2O$	Thioacetamide L-cysteine Thiourea	L-cysteine: irregular nanoparticles Thiourea: nanowires with diameters of about 200–300 nm	-	Electro-chemical measurements	Liu et al. (2018)

(Continued on following page)

TABLE 2 | (*Continued*) Summary of previous work on the effect of anions on the morphology, particle size, and crystal structure of various chalcogenides.

No	Materials	Metal precursors	Sulfur precursors	Morphology and size	Crystal phase	Application	References
9	CdS synthesized *via* hydrothermal method	$Cd(NO_3)_2 4H_2O$	Thiourea Thioacetamide L-cysteine	Thiourea: dendritic-like Architecture with diameter and length of the trunk are 0.3 and 2.5 μm, respectively Rod-like Morphology	Thiourea and L-cysteine: hexagonal Thioacetamide: mixture of hexagonal and metastable cubic CdS	Photocatalytic hydrogen production	Li et al. (2018)
10	CdS synthesized *via* solvothermal method	$Cd(NO_3)_2 4H_2O$ $Cd(CH_3COO)_2 \cdot 2H_2O$	Thiourea	Nanorods with diameter of around 10–20 nm Flower-like morphology with the diameter of around 30–40 nm Elemental sulphur: irregular structures at the base of the nanobars	Zinc blende Wurtzite	Photocatalytic degradation of methylene blue, methyl orange, safranin O, rhodamine B and remazol brilliant yellow	Malik et al. (2016)
11	Ag-modified CdS synthesized *via* solvothermal method	$CdCl_2$ $Ag(CH_3COO)$	Elemental sulphur, thiourea and L-cysteine	Thiourea: spherical-like structures forming globular aggregates L-cysteine: filamentous structures and lamellar aggregates	Hexagonal	Photocatalytic production of H_2	Soto Morillo et al. (2020)
12	ZnS synthesized *via* hydrothermal method	Zinc acetate Zinc nitrate	Thiourea Sodium sulphide	$Zn(NO_3)_2$ and thiourea: ~400 nm nanobelts $Zn(CH_3COO)_2$ and Na_2S: spheroidal and cuboidal shaped ZnS with average size of average size ~100–200 nm	$Zn(NO_3)_2$ and thiourea: wurtzite $Zn(CH_3COO)_2$ and Na_2S: Zinc blende	Photocatalytic degradation of methylene blue	Kanti Kole et al. (2014)
13	CdS synthesized in a hot-paraffin matrix	Cadmium stearate	Tributyl-phosphine sulfide Elemental sulfur Ammonium sulphide	Quantum dots with mean diameter of 3.67 (±0.27) nm	N Amorphous sphalerite structure	-	Yordanov et al. (2006)
14	CdS synthesized via chemical precipitation	Cadmium nitrate	Hydrogen sulphide Sodium sulphide	Spherical quantum dots with particle size less than 10 nm	Wurtzite and zinc blende	Photocatalytic degradation of Acid Blue-29	Qutub et al. (2016)
15	$CuInS_2$	bis (2-hyroxyacetophenato) copper (II)	Thioacetamide Thiourea L-cysteine Carbon disulfide Thiosemi-carbazide Thioglycolic acid Ammonium sulfide Sodium sulfite	When carbon disulfide was used instead of thioacetamide in the formation of $CuInS_2$ in ethylene glycol, irregular plate-like and bulky particles were achieved	Tetragonal	-	Sabet et al. (2013)

very slow in comparison to that from thioacetamide because of the strong coupling between the $-NH_2$ group and the nanoparticles. The ZnS nanostructures prepared using thiourea as a sulfur source had a cauliflower-like morphology with an average diameter of 0.8–1 μm. When sodium sulfide was used as the sulfur source, rice grain-shaped microstructures were produced while thioacetamide produces hedge apple-like shape with an average diameter of 1–2 μm.

In another study, Kozhevnikova et al. (2020) have successfully synthesized ZnS using the chemical bath deposition method. In this study, they have used different sources of sulfur including thiourea, thioacetamide, sodium thiosulfate, and sodium sulphide. All the synthesized ZnS exhibited wurtzite and sphalerite ZnS structures. In addition to this, they have also reported that the chemical nature and initial concentrations of $ZnSO_4$ and $ZnCl_2$ salts have no significant effect on particle size, phase composition, and crystal structure of ZnS colloids. FeS_2 with different morphologies have been successfully synthesized *via* solvothermal method as reported by Kar and Chaudhuri (2004) They found that the anions of the iron source ($FeSO_4 \cdot 7H_2O$, $FeCl_3$ and $Fe(NO_3)_3 \cdot 9H_2O$), temperature, and the molar concentrations of the precursors in the solvent play an important role in controlling the morphology of the FeS_2. When $FeSO_4 \cdot 7H_2O$ was used as the iron source, short nanorods having lengths up to 500 nm and diameter within 40–100 nm were produced. When $FeCl_3$ was used, large FeS_2 nanowires along

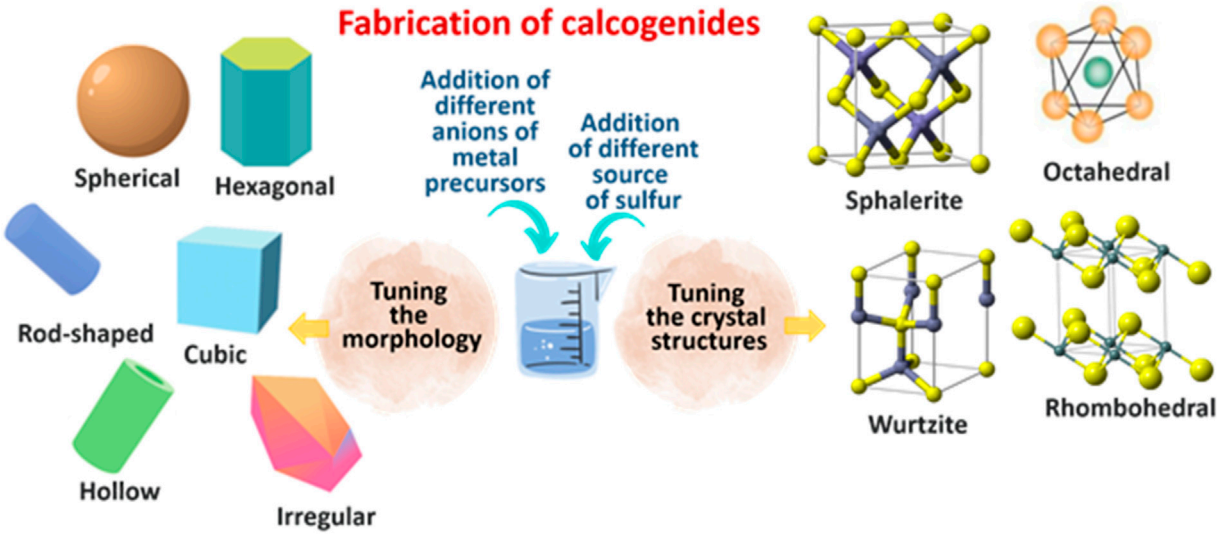

FIGURE 3 | Different morphologies and crystal structures of chalcogenides synthesized using different anion metal precursors and different sources of sulfur.

with some micro-rods were observed. When $Fe(NO_3)_3{\cdot}9H_2O$ was used as the precursor, uniform nanowires with diameters in the range 40–60 nm and length up to tens of μm.

Liu et al. (2018) reported that the different sources of sulfur in synthesizing MoS_2/Ni_3S_2 heterostructure have a significant influence on its structures and morphologies. They reported that MoS_2/Ni_3S_2 prepared from thioacetamide showed Ni_3S_2 nanorods and small MoS_2 nanosheets while L-cysteine showed the formation of irregular nanoparticles. In addition, nanowires with diameters of about 200–300 nm were observed when MoS_2/Ni_3S_2 prepared from thiourea. The thioacetamide-assisted synthesis of MoS_2/Ni_3S_2 showed superior H_2 evolution reaction activities due to the higher content of MoS_2 and it exhibited a larger electrochemically active surface area which provides more active sites for the H_2 evolution reaction. Li et al. (2018) have also reported the effects of these sulfur sources (thiourea, thioacetamide, and L-cysteine) on the properties of the resulted CdS including the crystal structure, morphology, and photocatalytic performance for H_2 evolution reaction. Based on their study, CdS prepared using thiourea with hexagonal branched dendritic structure has the smallest interfacial electron transfer resistance and the most negative conduction band bottom, and consequently shows the highest H_2 evolution reaction. CdS prepared using thioacetamide on the other hand exhibited a mixed phase of hexagonal and cubic which facilitated the recombination of photogenerated charge carriers that leads to a considerably lower H_2 evolution performance in comparison to CdS synthesized using thiourea. Moreover, low crystallized hexagonal CdS nanoparticles with no specific morphology were observed for CdS prepared using L-cysteine as the source of sulfur showed the largest interfacial electron transfer resistance and this resulted in the lowest H_2 evolution reaction.

Kanti Kole et al. (2014) have been successfully synthesized ZnS nanostructures of different morphologies, such as block-like, belt-like, spheroidal, and cuboidal shaped nanoparticles by using the simple hydrothermal technique. It has been shown that controlling the amount of sulphur precursor or utilizing different types and ratios of zinc and sulphur precursors can easily alter both the phase and morphology of ZnS nanostructures. They also reported that pure phase wurtzite ZnS nanobelts exhibited superior performance for the degradation of methylene blue dye with a degradation efficiency of 98% within 40 min of UV light irradiation. Different crystal structures of CdS nanoparticles prepared *via* chemical precipitation method using different sulfur sources ($(NH_4)_2S$, H_2S, Na_2S) have been reported by Qutub *et al.* Their group has studied the effect of different sulfur sources on the size of nanoparticles, respective band gaps, and crystalline structure. Based on their findings, a smaller particles size for CdS prepared using Na_2S, followed by H_2S and $(NH_4)_2S$ was observed, and the quantization in the band gap was directly in correlation with decreased particle size effects. Moreover, a mixed-phase of wurtzite and zinc-blende was obtained for CdS synthesized H_2S, while the pure phase of zinc-blende and wurtzite was obtained with Na_2S and $(NH_4)_2S$, respectively. They also reported that CdS synthesized using Na_2S with the addition of sodium hydroxide and methanol exhibited the highest activity and almost completely decolorized the derivative Acid Blue-29 under irradiation of visible light within 90 min. Tang et al. (2015) reported a one-pot synthesis of $CuInS_2$ using different anions to engineer their morphology and crystal structure. $CuInS_2$ having chalcopyrite, zinc blende, and wurtzite phases have been successfully synthesized by carefully selecting anions in metal precursors and manipulating reaction parameters such as reactant molar ratios and reaction temperature. They reported that $CuInS_2$ nanoplates with a wurtzite-zinc blende polytypism structure are formed in the presence of Cl^- ions. Furthermore, they also reported that the optical absorption measurements of $CuInS_2$

exhibited a strong dependence on the crystal structure and size.

Generally, the preparation methods and the conditions of synthesis are crucial factors for fabricating chalcogenides, and they possess a major role in the chemical as well as structural applications of chalcogenides. In addition to that, the influence of utilizing different anionic metal precursors and/or different sources of sulfur on the structural and morphological properties of chalcogenides was not largely reported in comparison to other semiconductors. Chalcogenides with controllable crystal structures and morphologies have potential applications in various areas as diverse as catalysis, plasmonics, sensing/imaging, spectroscopy, and medicine.

CHALLENGES DURING THE SYNTHESIS AND CRYSTAL GROWTH OF SEMICONDUCTORS

Properties of metal oxides have been considered to be dependent on the morphologies. However, in order to produce targeted shapes of a metal oxide, some agents should be employed in the synthesis. Therefore, metal oxides with different morphologies without the use of agents have become a major challenge. Fabrication of chalcogenides, in particular, can be quite challenging because of their stability. In addition to that, the selection of a suitable precursor is a crucial stage because it will not only have an influence on the physical properties of the materials but also its chemical and optical properties. Moreover, it is also important to avoid the use of toxic precursors, environmentally friendly solvents, keeping the reaction temperature close to room temperature, and also minimizing the quantities of generated by-products are great advantages that make the synthesis of metal oxides and chalcogenides outstanding.

FUTURE PROSPECTS

Controlled crystal growth of semiconductors is crucial for activity efficiency in various applications (biological, environmental, and energy). The controlled crystal growth can be achieved by changing the anion precursor salts and keeping other conditions the same. However, to date, the reports on this matter are still less in number in which some research gaps are yet to be answered. The following are the future prospects that should be considered and addressed:

- Most of the syntheses using different anion precursors to produce different shapes require different synthesis conditions. In order to effectively study the role of anions, one should keep other conditions the same and vary the anion precursors only.
- Most syntheses and studies still require stabilizing and capping agents to aid the formation of different morphologies of a semiconductor.
- In-depth study of crystallographic properties of a semiconductor should be carried out to study the overall effect of different anions on a semiconductor.
- Deeper understanding of the growth mechanisms of the semiconductor *via* computational simulation would help the researchers to fabricate materials with desired properties more efficiently.

CONCLUSION

Various morphologies of semiconductors (metal oxides and chalcogenides) have been obtained using different anion precursor salts through typical synthesis methods. Spherical particles are normally observed due to their thermodynamically favorable properties. However, by changing the anion precursor's salts, the morphology of a semiconductor is affected accordingly. This can be said that the anions have some effects on the final forms of a semiconductor. Nevertheless, in-depth studies are required to investigate the effect of anions on the crystal growth of a semiconductor to get maximum efficiency for the fabricated particles.

AUTHOR CONTRIBUTIONS

SM: writing–original draft. AR: writing–original draft. MK: supervision, funding acquisition, writing–review and editing.

FUNDING

The authors would like to acknowledge the FIC block grant UBD/RSCH/1.4/FICBF(b)/2021/035 received from Universiti Brunei Darussalam, Brunei Darussalam.

ACKNOWLEDGMENTS

The authors would like to acknowledge the Universiti Brunei Darussalam, Brunei Darussalam for all type of support.

REFERENCES

Aboul-Gheit, A. K., El-Desouki, D. S., and El-Salamony, R. A. (2014). Different Outlet for Preparing Nano-TiO2 Catalysts for the Photodegradation of Black B Dye in Water. *Egypt. J. Pet.* 23 (3), 339–348. doi:10.1016/j.ejpe.2014.08.010

Ahluwalia, G. K. (2017). Applications of Chalcogenides: S, Se, and Te. doi:10.1007/978-3-319-41190-3

Aneggi, E., Wiater, D., de Leitenburg, C., Llorca, J., and Trovarelli, A. (2014). Shape-Dependent Activity of Ceria in Soot Combustion. *ACS Catal.* 4 (1), 172–181. doi:10.1021/cs400850r

Benhammada, A., Trache, D., Kesraoui, M., Tarchoun, A. F., Chelouche, S., and Mezroua, A. (2020). Synthesis and Characterization of α-Fe2O3 Nanoparticles from Different Precursors and Their Catalytic Effect on the thermal Decomposition of Nitrocellulose. *Thermochim. Acta* 686 (February), 178570. doi:10.1016/j.tca.2020.178570

Bhosale, R., Kumar, A., AlMomani, F., Ghosh, U., Saad Anis, M., Kakosimos, K., et al. (2016). Solar Hydrogen Production via a Samarium Oxide-Based Thermochemical Water Splitting Cycle. *Energies* 9 (5), 316. doi:10.3390/en9050316

Cao, S., Tao, F., Tang, Y., Li, Y., and Yu, J. (2016). Size- and Shape-dependent Catalytic Performances of Oxidation and Reduction Reactions on Nanocatalysts. *Chem. Soc. Rev.* 45, 4747–4765. doi:10.1039/c6cs00094k

Chen, C., Zhan, Y., Li, D., Zhang, Y., Lin, X., Jiang, L., et al. (2018). Preparation of CuO/CeO2 Catalyst with Enhanced Catalytic Performance for Water-Gas Shift Reaction in Hydrogen Production. *Energy Technol.* 6 (6), 1096–1103. doi:10.1002/ente.201700750

Chen, J., Shen, S., Wu, P., and Guo, L. (2015). Nitrogen-doped CeOx Nanoparticles Modified Graphitic Carbon Nitride for Enhanced Photocatalytic Hydrogen Production. *Green. Chem.* 17 (1), 509–517. doi:10.1039/c4gc01683a

Chiu, C.-Y., Chung, P.-J., Lao, K.-U., Liao, C.-W., and Huang, M. H. (2012). Facet-Dependent Catalytic Activity of Gold Nanocubes, Octahedra, and Rhombic Dodecahedra toward 4-Nitroaniline Reduction. *J. Phys. Chem. C* 116 (44), 23757–23763. doi:10.1021/jp307768h

Cho, S., Jung, S.-H., and Lee, K.-H. (2008). Morphology-Controlled Growth of ZnO Nanostructures Using Microwave Irradiation: From Basic to Complex Structures. *J. Phys. Chem. C* 112 (33), 12769–12776. doi:10.1021/jp803783s

C. Nehru, L., Swaminathan, V., and Sanjeeviraja, C. (2012). Photoluminescence Studies on Nanocrystalline Tin Oxide Powder for Optoelectronic Devices. *Materials* 2 (2), 6–10. doi:10.5923/j.materials.20120202.02

Dey, S., Das, S., and Kar, A. K. (2021). Role of Precursor Dependent Nanostructures of ZnO on its Optical and Photocatalytic Activity and Influence of FRET between ZnO and Methylene Blue Dye on Photocatalysis. *Mater. Chem. Phys.* 270, 124872. doi:10.1016/j.matchemphys.2021.124872

Feng, G., Han, W., Wang, Z., Li, F., and Xue, W. (2018). Highly Reducible Nanostructured CeO2 for CO Oxidation. *Catalysts* 8 (11), 535. doi:10.3390/catal8110535

Gaur, R., and Jeevanandam, P. (2015). Effect of Anions on the Morphology of CdS Nanoparticles Prepared via Thermal Decomposition of Different Cadmium Thiourea Complexes in a Solvent and in the Solid State. *New J. Chem.* 39 (12), 9442–9453. doi:10.1039/C5NJ01605C

Gowthaman, N. S. K., Ngee Lim, H., Balakumar, V., and Shankar, S. (2020). Ultrasonic Synthesis of CeO2@organic Dye Nanohybrid: Environmentally Benign Rabid Electrochemical Sensing Platform for Carcinogenic Pollutant in Water Samples. *Ultrason. Sonochem.* 61, 104828. doi:10.1016/j.ultsonch.2019.104828

Guo, K., Li, H., and Yu, Z. (2018). Size-Dependent Catalytic Activity of Monodispersed Nickel Nanoparticles for the Hydrolytic Dehydrogenation of Ammonia Borane. *ACS Appl. Mater. Inter.* 10 (1), 517–525. doi:10.1021/acsami.7b14166

Guru, S., Mishra, D., Singh, M., Amritphale, S. S., and Joshi, S. (2016). Effect of SO4 2-, Cl- and NO3 - Anions on the Formation of Iron Oxide Nanoparticles via Microwave Synthesis. *Prot. Met. Phys. Chem. Surf.* 52 (4), 627–631. doi:10.1134/S2070205116040146

Gusatti, M., Barroso, G. S., Campos, C. E. M. d., Souza, D. A. R. d., Rosário, J. d. A. d., Lima, R. B., et al. (2011). Effect of Different Precursors in the Chemical Synthesis of ZnO Nanocrystals. *Mat. Res.* 14 (2), 264–267. doi:10.1590/S1516-14392011005000035

Hasnidawani, J. N., Azlina, H. N., Norita, H., Bonnia, N. N., Ratim, S., and Ali, E. S. (2016). Synthesis of ZnO Nanostructures Using Sol-Gel Method. *Proced. Chem.* 19, 211–216. doi:10.1016/j.proche.2016.03.095

He, K., Li, J., Shen, Y., and Yu, Y. (2019). pH-Responsive Polyelectrolyte Coated Gadolinium Oxide-Doped Mesoporous Silica Nanoparticles (Gd2O3@MSNs) for Synergistic Drug Delivery and Magnetic Resonance Imaging Enhancement. *J. Mater. Chem. B* 7 (43), 6840–6854. doi:10.1039/c9tb01654f

Herricks, T., Chen, J., and Xia, Y. (2004). Polyol Synthesis of Platinum Nanoparticles: Control of Morphology with Sodium Nitrate. *Nano Lett.* 4 (12), 2367–2371. doi:10.1021/nl048570a

Hussain, M., Ibupoto, Z. H., Abbasi, M. A., Nur, O., and Willander, M. (2014). Effect of Anions on the Morphology of Co3O4 Nanostructures Grown by Hydrothermal Method and Their pH Sensing Application. *J. Electroanalytical Chem.* 717-718 (717), 78–82. doi:10.1016/j.jelechem.2014.01.011

Jain, S., Panigrahi, A., and Sarma, T. K. (2019). Counter Anion-Directed Growth of Iron Oxide Nanorods in a Polyol Medium with Efficient Peroxidase-Mimicking Activity for Degradation of Dyes in Contaminated Water. *ACS Omega* 4 (8), 13153–13164. doi:10.1021/acsomega.9b01201

Jayakumar, G., Albert Irudayaraj, A., Dhayal Raj, A., John Sundaram, S., and Kaviyarasu, K. (2022). Electrical and Magnetic Properties of Nanostructured Ni Doped CeO2 for Optoelectronic Applications. *J. Phys. Chem. Sol.* 160 (August), 110369. doi:10.1016/j.jpcs.2021.110369

Kaenphakdee, S., Putthithanas, P., Yodyingyong, S., Leelawattanachai, J., Triampo, W., Sanpo, N., et al. (2022). Zinc Oxide Synthesis from Extreme Ratios of Zinc Acetate and Zinc Nitrate: Synergistic Morphology. *Materials* 15 (2), 570. doi:10.3390/ma15020570

Kanti Kole, A., Sekhar Tiwary, C., and Kumbhakar, P. (2014). Morphology Controlled Synthesis of Wurtzite ZnS Nanostructures through Simple Hydrothermal Method and Observation of White Light Emission from ZnO Obtained by Annealing the Synthesized ZnS Nanostructures. *J. Mater. Chem. C* 2 (21), 4338–4346. doi:10.1039/C4TC00091A

Kar, S., and Chaudhuri, S. (2004). Solvothermal Synthesis of Nanocrystalline FeS2 with Different Morphologies. *Chem. Phys. Lett.* 398 (1–3), 22–26. doi:10.1016/j.cplett.2004.09.028

Kathalingam, A., Park, H.-C., Kim, S.-D., Kim, H.-S., Velumani, S., and Mahalingam, T. (2015). Synthesis of ZnO Nanorods Using Different Precursor Solutions and Their Two Terminal Device Characterization. *J. Mater. Sci. Mater. Electron.* 26 (8), 5724–5734. doi:10.1007/s10854-015-3129-6

Khan, M. E., Khan, M. M., and Cho, M. H. (2017). Ce3+-ion, Surface Oxygen Vacancy, and Visible Light-Induced Photocatalytic Dye Degradation and Photocapacitive Performance of CeO2-Graphene Nanostructures. *Sci. Rep.* 7 (1), 1–17. doi:10.1038/s41598-017-06139-6

Khan, M. M. (2021). in *Chalcogenide-Based Nanomaterials as Photocatalysts*. Editor M. M. Khan (Amsterdam, Netherlands: Elsevier). doi:10.1016/C2019-0-01819-5

Khodashenas, B., and Ghorbani, H. R. (2019). Synthesis of Silver Nanoparticles with Different Shapes. *Arabian J. Chem.* 12 (8), 1823–1838. doi:10.1016/j.arabjc.2014.12.014

Kim, Y., Amaranatha Reddy, D., Park, H., and Kim, T. K. (2016). Anionic Precursor-Mediated Morphology-Controlled Synthesis of ZnS Nanostructures: Morphology-dependent Tunable Photoluminescence in the Visible Region and Pulsed Laser-Induced Efficient Reduction of Cr(VI). *Ceramics Int.* 42 (10), 12046–12054. doi:10.1016/j.ceramint.2016.04.132

Koutavarapu, R., Tamtam, M. R., Rao, M. C., Peera, S. G., and Shim, J. (2021). Recent Progress in Transition Metal Oxide/Sulfide Quantum Dots-Based Nanocomposites for the Removal of Toxic Organic Pollutants. *Chemosphere* 272, 129849. doi:10.1016/j.chemosphere.2021.129849

Kowsari, E., Pradhan, D., and Sohn, Y. (2017). "Carbon-Based Nanocomposites for Visible Light-Induced Photocatalysis," in *Nanocomposites for Visible Light-Induced Photocatalysis*, 203–249. doi:10.1007/978-3-319-62446-4_8

Kozhevnikova, N. S., Maskaeva, L. N., Markov, V. F., and Vorokh, A. S. (2020). Effect of Chemical Reaction Mechanism on the Formation of ZnS Colloid Particles with Structure Disordering. *Mater. Sci. Semiconductor Process.* 113, 105047. doi:10.1016/j.mssp.2020.105047

Kuan, W.-F., Yu, W.-Y., Tu, F.-Y., Chung, C.-H., Chang, Y.-C., Lin, M. M., et al. (2022). Facile Reflux Preparation of Defective Mesoporous Ceria Nanorod with Superior Catalytic Activity for Direct Carbon Dioxide Conversion into Dimethyl Carbonate. *Chem. Eng. J.* 430 (P1), 132941. doi:10.1016/j.cej.2021.132941

Kumar, A., Sharma, M., Gautam, R. K., Agarwala, P., and Basu, S. (2017). Synthesis of Mesoporous Cerium Oxide (CeO2) Nanoparticles and Effect of Cerium Precursors on Transamidation of Acetamide with N-Octylamine under Solvent-free Conditions. *j nanosci nanotechnol* 17 (7), 4983–4988. doi:10.1166/jnn.2017.13744

Li, H., Liu, L., Wang, Z., Zheng, X., Meng, S., Chen, S., et al. (2018). Optimizing the Precursor of Sulfur Source for Hydrothermal Synthesis of High Performance CdS for Photocatalytic Hydrogen Production. *RSC Adv.* 8 (21), 11489–11497. doi:10.1039/C8RA00250A

Li, J., and Wu, N. (2015). Semiconductor-Based Photocatalysts and Photoelectrochemical Cells for Solar Fuel Generation: A Review. *Catal. Sci. Technol.* 5, 1360–1384. doi:10.1039/c4cy00974f

Lin, C.-Y., Zhang, J., and Xia, Z. (2019). Coordination-Dependent Catalytic Activity and Design Principles of Metal-Organic Frameworks as Efficient Electrocatalysts for Clean Energy Conversion. *J. Phys. Chem. C* 123 (1), 214–221. doi:10.1021/acs.jpcc.8b10375

Liu, B., Zhao, X., Terashima, C., Fujishima, A., and Nakata, K. (2014). Thermodynamic and Kinetic Analysis of Heterogeneous Photocatalysis for Semiconductor Systems. *Phys. Chem. Chem. Phys.* 16, 8751–8760. doi:10.1039/c3cp55317e

Liu, X., Wang, P., Zhang, Q., Huang, B., Wang, Z., Liu, Y., et al. (2018). Synthesis of MoS2/Ni3S2 Heterostructure for Efficient Electrocatalytic Hydrogen Evolution Reaction through Optimizing the Sulfur Sources Selection. *Appl. Surf. Sci.* 459, 422–429. doi:10.1016/j.apsusc.2018.08.024

Loh, J. Y. Y., and Kherani, N. P. (2019). X-Ray Photospectroscopy and Electronic Studies of Reactor Parameters on Photocatalytic Hydrogenation of Carbon Dioxide by Defect-Laden Indium Oxide Hydroxide Nanorods. *Molecules* 24 (3818), 3818. doi:10.3390/molecules24213818

Malik, R., Singh, C., Garg, R., Kumar, V., and Singhal, S. (2016). Morphology Controlled CdS Nanostructures: A Proficient Visible-Light-Driven Photocatalyst. *Anal. Chem. Lett.* 6 (5), 492–507. doi:10.1080/22297928.2016.1241718

Mallakpour, S., Nikkhoo, E., and Hussain, C. M. (2022). Application of MOF Materials as Drug Delivery Systems for Cancer Therapy and Dermal Treatment. *Coord. Chem. Rev.* 451, 214262. doi:10.1016/j.ccr.2021.214262

Matussin, S., Harunsani, M. H., Tan, A. L., and Khan, M. M. (2020). Plant-Extract-Mediated SnO2 Nanoparticles: Synthesis and Applications. *ACS Sustain. Chem. Eng.* 8 (8), 3040–3054. doi:10.1021/acssuschemeng.9b06398

Matussin, S. N., Harunsani, M. H., Tan, A. L., Mohammad, A., Cho, M. H., and Khan, M. M. (2020). Photoantioxidant Studies of SnO2 Nanoparticles Fabricated Using Aqueous Leaf Extract of Tradescantia Spathacea. *Solid State. Sci.* 105, 106279. doi:10.1016/j.solidstatesciences.2020.106279

Mishra, S. B., and Nanda, B. R. K. (2020). Facet Dependent Catalytic Activities of Anatase TiO2 for CO2 Adsorption and Conversion. *Appl. Surf. Sci.* 531, 147330. doi:10.1016/j.apsusc.2020.147330

M.S, R., Shanmuga Priya, S., Freudenberg, N. C., Sudhakar, K., and Tahir, M. (2021). Metal-Organic Framework-Based Photocatalysts for Carbon Dioxide Reduction to Methanol: A Review on Progress and Application. *J. CO2 Utilization* 43, 101374. doi:10.1016/j.jcou.2020.101374

Naidi, S. N., Khan, F., Tan, A. L., Harunsani, M. H., Kim, Y.-M., and Khan, M. M. (2021). Photoantioxidant and Antibiofilm Studies of green Synthesized Sn-Doped CeO2 Nanoparticles Using Aqueous Leaf Extracts of Pometia Pinnata. *New J. Chem.* 45 (17), 7816–7829. doi:10.1039/D1NJ00416F

Navya, P. N., and Daima, H. K. (2016). Rational Engineering of Physicochemical Properties of Nanomaterials for Biomedical Applications with Nanotoxicological Perspectives. *Nano Convergence* 3 (1). doi:10.1186/s40580-016-0064-z

Nicholas, N. J., Franks, G. v., and Ducker, W. A. (2012). Selective Adsorption to Particular Crystal Faces of ZnO. *Langmuir* 28 (18), 7189–7196. doi:10.1021/la2050674

Ozel, E., Tuncolu, I. G., Tuncolu, I. G., Aciksari, C., and Suvaci, E. (2016). Effect of Precursor Type on Zinc Oxide Formation and Morphology Development during Hydrothermal Synthesis. *Hittite J. Sci. Eng.* 3 (2), 73–80. doi:10.17350/HJSE19030000034

Panda, N. R., Acharya, B. S., and Nayak, P. (2013). Sonochemical Synthesis of Nitrogen Doped ZnO Nanorods: Effect of Anions on Growth and Optical Properties. *J. Mater. Sci. Mater. Electron.* 24 (10), 4043–4049. doi:10.1007/s10854-013-1359-z

Parwaiz, S., Khan, M. M., and Pradhan, D. (2019). CeO2-based Nanocomposites: An Advanced Alternative to TiO2 and ZnO in Sunscreens. *mat express* 9 (3), 185–202. doi:10.1166/mex.2019.1495

Popescu, M. (2006). Chalcogenides - Past, Present, Future. *J. Non-Crystalline Sol.* 352, 887–891. doi:10.1016/j.jnoncrysol.2005.11.126

Pourrahimi, A. M., Liu, D., Pallon, L. K. H., Andersson, R. L., Martínez Abad, A., Lagarón, J.-M., et al. (2014). Water-based Synthesis and Cleaning Methods for High Purity ZnO Nanoparticles - Comparing Acetate, Chloride, Sulphate and Nitrate Zinc Salt Precursors. *RSC Adv.* 4 (67), 35568–35577. doi:10.1039/c4ra06651k

Qi, K., Qin, Q., Duan, X., Wang, G., Wu, L., and Zheng, W. (2014). Geometric Matching Principle for Adsorption Selectivity of Ionic Liquids: A Simple Method into the Fascinating World of Shape-Controlled Chemistry. *Chem. Eur. J.* 20 (29), a–n. doi:10.1002/chem.201400409

Qi, K., Yang, J., Fu, J., Wang, G., Zhu, L., Liu, G., et al. (2013). Morphology-Controllable ZnO Rings: Ionic Liquid-Assisted Hydrothermal Synthesis, Growth Mechanism and Photoluminescence Properties. *CrystEngComm* 15 (34), 6729–6735. doi:10.1039/c3ce27007f

Qutub, N., Pirzada, B. M., Umar, K., and Sabir, S. (2016). Synthesis of CdS Nanoparticles Using Different Sulfide Ion Precursors: Formation Mechanism and Photocatalytic Degradation of Acid Blue-29. *J. Environ. Chem. Eng.* 4 (1), 808–817. doi:10.1016/j.jece.2015.10.031

Rahman, A., Harunsani, M. H., Tan, A. L., Ahmad, N., and Khan, M. M. (2021). Antioxidant and Antibacterial Studies of Phytogenic Fabricated ZnO Using Aqueous Leaf Extract of Ziziphus Mauritiana Lam. *Chem. Pap.* 75, 3295–3308. doi:10.1007/s11696-021-01553-7

Rahman, A., and Khan, M. M. (2021). Chalcogenides as Photocatalysts. *New J. Chem.* 45, 19622–19635. doi:10.1039/D1NJ04346C

Sabet, M., Salavati-Niasari, M., Ghanbari, D., Amiri, O., and Yousefi, M. (2013). Synthesis of CuInS2 Nanoparticles via Simple Microwave Approach and Investigation of Their Behavior in Solar Cell. *Mater. Sci. Semiconductor Process.* 16 (3), 696–704. doi:10.1016/j.mssp.2012.12.011

Sahay, P. P., Mishra, R. K., Pandey, S. N., Jha, S., and Shamsuddin, M. (2013). Structural, Dielectric and Photoluminescence Properties of Co-precipitated Zn-Doped SnO2 Nanoparticles. *Curr. Appl. Phys.* 13 (3), 479–486. doi:10.1016/j.cap.2012.09.010

Samiee, S., and Goharshadi, E. K. (2012). Effects of Different Precursors on Size and Optical Properties of Ceria Nanoparticles Prepared by Microwave-Assisted Method. *Mater. Res. Bull.* 47 (4), 1089–1095. doi:10.1016/j.materresbull.2011.12.058

Sanjini, N. S., Winston, B., and Velmathi, S. (2017). Effect of Precursors on the Synthesis of CuO Nanoparticles under Microwave for Photocatalytic Activity towards Methylene Blue and Rhodamine B Dyes. *J. Nanosci Nanotechnol* 17 (1), 495–501. doi:10.1166/jnn.2017.11785

Segets, D., Marczak, R., Schäfer, S., Paula, C., Gnichwitz, J.-F., Hirsch, A., et al. (2011). Experimental and Theoretical Studies of the Colloidal Stability of Nanoparticles–A General Interpretation Based on Stability Maps. *ACS Nano* 5 (6), 4658–4669. doi:10.1021/nn200465b

Shi, Y., Yang, A.-F., Cao, C.-S., and Zhao, B. (2019). Applications of MOFs: Recent Advances in Photocatalytic Hydrogen Production from Water. *Coord. Chem. Rev.* 390, 50–75. doi:10.1016/j.ccr.2019.03.012

Siegfried, M. J., and Choi, K.-S. (2005). Directing the Architecture of Cuprous Oxide Crystals during Electrochemical Growth. *Angew. Chem. Int. Ed.* 44 (21), 3218–3223. doi:10.1002/anie.200463018

Singh, P. K., Mukherjee, S., Ghosh, C. K., and Maitra, S. (2017). Influence of Precursor Type on Structural, Morphological, Dielectric and Magnetic Properties of TiO2 Nanoparticles. *Cerâmica* 63 (368), 549–556. doi:10.1590/0366-69132017633682145

Soren, S., Jena, S. R., Samanta, L., and Parhi, P. (2015). Antioxidant Potential and Toxicity Study of the Cerium Oxide Nanoparticles Synthesized by Microwave-Mediated Synthesis. *Appl. Biochem. Biotechnol.* 177 (1), 148–161. doi:10.1007/s12010-015-1734-8

Soto Morillo, E., Mota Toledo, N., García Fierro, J. L., and Navarro Yerga, R. M. (2020). Role of the Sulphur Source in the Solvothermal Synthesis of Ag-CdS Photocatalysts: Effects on the Structure and Photoactivity for Hydrogen Production. *Hydrogen* 1 (1), 64–89. doi:10.3390/hydrogen1010005

Sun, D., Wong, M., Sun, L., Li, Y., Miyatake, N., and Sue, H.-J. (2007). Purification and Stabilization of Colloidal ZnO Nanoparticles in Methanol. *J. Sol-gel Sci. Technol.* 43 (2), 237–243. doi:10.1007/s10971-007-1569-z

Sun, Z., Wu, X., Guan, D., Chen, X., Dai, J., Gu, Y., et al. (2021). One Pot-Synthesized Ag/Ag-Doped CeO2 Nanocomposite with Rich and Stable 3D Interfaces and Ce3+ for Efficient Carbon Dioxide Electroreduction. *ACS Appl. Mater. Inter.* 13, 59993–60001. doi:10.1021/acsami.1c19529

Tang, A., Hu, Z., Yin, Z., Ye, H., Yang, C., and Teng, F. (2015). One-pot Synthesis of CuInS2 Nanocrystals Using Different Anions to Engineer Their Morphology and crystal Phase. *Dalton Trans.* 44 (19), 9251–9259. doi:10.1039/c5dt01111f

van Rijt, M. M. J., Oosterlaken, B. M., Joosten, R. R. M., Wijkhuijs, L. E. A., Bomans, P. H. H., Friedrich, H., et al. (2020). Counter-Ion Influence on the Mechanism of HMTA-Mediated ZnO Formation. *CrystEngComm* 22 (35), 5854–5861. doi:10.1039/d0ce00847h

Wang, H., Liu, Y., Li, M., Huang, H., Xu, H. M., Hong, R. J., et al. (2010). Multifunctional TiO2nanowires-Modified Nanoparticles Bilayer Film for 3D Dye-Sensitized Solar Cells. *Optoelectronics Adv. Mater. Rapid Commun.* 4 (8), 1166–1169. doi:10.1039/b000000x

Wang, Y., Chen, W., Chen, X., Feng, H., Shen, D., Huang, B., et al. (2018). Effect of Sulfur Source on Photocatalytic Degradation Performance of CdS/MoS2 Prepared with One-step Hydrothermal Synthesis. *J. Environ. Sci.* 65, 347–355. doi:10.1016/j.jes.2017.07.004

Wu, Q., Zhang, F., Xiao, P., Tao, H., Wang, X., Hu, Z., et al. (2008). Great Influence of Anions for Controllable Synthesis of CeO2 Nanostructures: From Nanorods to Nanocubes. *J. Phys. Chem. C* 112 (44), 17076–17080. doi:10.1021/jp804140e

Yang, L., Chen, C., Rui, Z., and Ji, H. (2020). Anodic Aluminum Oxide Supported Pd@ CeO2 Catalyst for Organic Gas Pollutants Removal with an Enhanced Performance. *Catal. Today* 355 (March), 602–607. doi:10.1016/j.cattod.2019.04.065

Yang, S., and Gao, L. (2006). Controlled Synthesis and Self-Assembly of CeO2 Nanocubes. *J. Am. Chem. Soc.* 128 (29), 9330–9331. doi:10.1021/ja063359h

Yin, L., Zhang, D., Wang, D., Wang, F., Huang, J., Kong, X., et al. (2016). Controlled Synthesis of Sm2O3 Nano/microstructures with New Morphology by Hydrothermal-Calcination Process. *Ceramics Int.* 42 (10), 11998–12004. doi:10.1016/j.ceramint.2016.04.126

Yordanov, G. G., Adachi, E., and Dushkin, C. D. (2006). Growth Kinetics and Characterization of Fluorescent CdS Nanocrystals Synthesized with Different Sulfur Precursors in Paraffin Hot-Matrix. *Colloids Surf. A: Physicochemical Eng. Aspects* 289 (1–3), 118–125. doi:10.1016/j.colsurfa.2006.04.019

Zeng, X., Pramana, S. S., Batabyal, S. K., Mhaisalkar, S. G., Chen, X., and Jinesh, K. B. (2013). Low Temperature Synthesis of Wurtzite Zinc Sulfide (ZnS) Thin Films by Chemical Spray Pyrolysis. *Phys. Chem. Chem. Phys.* 15 (18), 6763. doi:10.1039/c3cp43470b

Zhang, X., Wei, Y., Song, Z., Liu, W., Gao, C., and Luo, J. (2021). Silicotungstic Acid Modified CeO2 Catalyst with High Stability for the Catalytic Combustion of Chlorobenzene. *Chemosphere* 263, 128129. doi:10.1016/j.chemosphere.2020.128129

Zhang, Z., Yue, C., and Hu, J. (2017). Fabrication of Porous MoS2 with Controllable Morphology and Specific Surface Area for Hydrodeoxygenation. *Nano* 12 (09), 1750116. doi:10.1142/S1793292017501168

Zhou, R., Zhou, R., Alam, D., Zhang, T., Li, W., Xia, Y., et al. (2021). Plasmacatalytic Bubbles Using CeO2 for Organic Pollutant Degradation. *Chem. Eng. J.* 403 (June), 126413. doi:10.1016/j.cej.2020.126413

Zhu, C., Wei, X., Li, W., Pu, Y., Sun, J., Tang, K., et al. (2020). Crystal-plane Effects of CeO2{110} and CeO2{100} on Photocatalytic CO2 Reduction: Synergistic Interactions of Oxygen Defects and Hydroxyl Groups. *ACS Sustain. Chem. Eng.* 8 (38), 14397–14406. doi:10.1021/acssuschemeng.0c04205

Conflict of Interest: The authors declare that the research was conducted in the absence of any commercial or financial relationships that could be construed as a potential conflict of interest.

Publisher's Note: All claims expressed in this article are solely those of the authors and do not necessarily represent those of their affiliated organizations or those of the publisher, the editors, and the reviewers. Any product that may be evaluated in this article, or claim that may be made by its manufacturer, is not guaranteed or endorsed by the publisher.